

Distribution-Aware GMD Transceiver Design for Probabilistic Shaping in MIMO

Tzu-Hsuan Chou, Chih-Hao Liu, and Jing Jiang

Abstract—Multiple-input multiple-output (MIMO) transceiver design and probabilistic shaping (PS) are key enablers for high spectral efficiency in 6G wireless networks. This work proposes a distribution-aware MIMO transceiver optimized for PS constellation symbols, including a Bayesian geometric-mean decomposition (BGMD) precoder and a maximum a posteriori-VBLAST (MAP-VBLAST) detector. BGMD precoder incorporates PS priors into the derivation and equalizes layer gains to facilitate a single modulation and coding scheme for low-complexity transmissions while preserving channel capacity. MAP-VBLAST leverages these PS priors for optimal MAP detection within a successive interference cancellation (SIC) framework. Furthermore, a new codeword-to-layer mapping scheme, termed layer-contained MIMO (LC-MIMO), is proposed. By containing each codeblock (CB) within a single layer, LC-MIMO enables SIC at CB level, allowing the receiver to exploit the error-correction capability of channel coding to mitigate error propagation. Numerical results show that the BGMD transceiver with LC-MIMO achieves notable performance gains over state-of-the-art methods.

Index Terms—GMD, UCD, Transceivers, Probabilistic Shaping

I. INTRODUCTION

The pursuit of higher spectral efficiency with reduced computational complexity has become a central objective in 6G wireless networks [1]. Probabilistic shaping (PS) and multiple-input multiple-output (MIMO) transceiver design are key enablers for closing the gap to information-theoretic limits. By tailoring the symbol distribution to approximate Gaussian inputs, PS enables communication systems to approach the Shannon channel capacity. This potential has motivated growing interest in integrating PS into modern wireless standards, including 5G New Radio (5G NR) [2], 6G, and Wi-Fi [3].

Conventional MIMO transceivers employ singular value decomposition (SVD)-based precoding to diagonalize the MIMO channel, but SVD could result in subchannels with unequal gains, which is undesirable for transmissions that employ a single modulation and coding scheme (MCS). In 5G NR, the codeword-to-layer (CW-to-layer) mapping distributes the bits of a codeblock (CB) across multiple spatial layers to exploit spatial diversity. However, when the subchannel gains are highly unequal, this CW-to-layer mapping in 5G NR significantly degrades channel coding performance, particularly at high code rates. To address this issue, geometric mean decomposition (GMD)-based transceivers [4], [5] have been proposed to transform the MIMO channel into parallel subchannels with identical gains, improving the decoding performance for

single-MCS transmission while preserving the Gaussian-input MIMO channel capacity. Despite its structural compatibility with the transmission of PS quadrature amplitude modulation (QAM) symbols, existing GMD-based transceiver designs are derived under the assumption of uniformly distributed QAM symbols and cannot exploit the non-uniform symbol statistics induced by PS, leading to a performance gap relative to the achievable capacity under PS QAM signaling.

Several recent works [2], [6]–[8] have investigated PS in multiple-antenna systems. The work [6] jointly optimizes PS constellation distributions and beamforming to maximize mutual information, but it is designed for multiple-input single-output systems. The work [7] focuses on achieving shaping and diversity gains in MIMO channels through signal space diversity. The work [2] investigates PS in 5G NR MIMO and demonstrates that PS can mitigate large signal-to-noise ratio (SNR) gaps between MCSs, improving the achievable throughput envelope. The work [8] studies PS symbols over MIMO channels using nonlinear sphere decoding [9], showing shaping gains beyond the 1.53 dB limit in additive white Gaussian noise (AWGN) channels. However, these works [2], [6]–[8] do not consider a MIMO transceiver optimized for the PS symbol distribution. Further work is required to develop a distribution-aware MIMO transceiver capable of fully harvesting the PS gains in spatial multiplexing.

This work proposes a distribution-aware MIMO transceiver that incorporates the PS symbol distribution as a statistical prior in the transceiver design. A maximum a posteriori (MAP) symbol detector is derived to exploit PS priors and is simplified into a VBLAST-like successive interference cancellation (SIC) framework, termed MAP-VBLAST. Building on this framework, a Bayesian GMD (BGMD) precoder is developed to embed PS priors into the channel decomposition process and equalize the subchannel gains under PS signaling. To mitigate the susceptibility of SIC to error propagation, a layer-contained MIMO (LC-MIMO) mapping scheme is proposed. LC-MIMO confines each codeblock (CB) to a single spatial layer, rather than distributing it across layers as in 5G NR, enabling SIC at the CB level. This allows the receiver to exploit the error-correction capability of channel coding, producing more reliable symbol estimates that mitigate error propagation in SIC. Numerical results show that the BGMD transceiver with LC-MIMO achieves substantial gains in both throughput and decoding performance compared with state-of-the-art methods.

Notation: Bold lowercase letters \mathbf{x} and bold uppercase letters \mathbf{X} denote vectors and matrices, respectively; \mathbf{X}^\top , \mathbf{X}^H , \mathbf{X}^{-1} denote the transpose, conjugate transpose, and inverse of

This work was supported by Qualcomm Wireless Research.

T.-H. Chou, C.-H. Liu and J. Jiang are with Qualcomm, Inc., San Diego, CA, USA; emails: {tzhuchou, chihliu, jingj}@qti.qualcomm.com

\mathbf{X} , respectively. \mathbf{I}_N denotes the $N \times N$ identity matrix.

II. SYSTEM MODEL

Section II-A introduces the signal model with linear MIMO precoding. Section II-B describes the probabilistic shaping method used for QAM symbol generation.

A. Signal Model

We consider a single-user MIMO downlink transmission with N_t transmit antennas and N_r receive antennas, employing spatial multiplexing with $L \leq \min(N_t, N_r)$ spatial layers. The received signal $\mathbf{y} \in \mathbb{C}^{N_r \times 1}$ is given by

$$\mathbf{y} = \mathbf{H}\mathbf{F}\mathbf{x} + \mathbf{n}, \quad (1)$$

where $\mathbf{H} \in \mathbb{C}^{N_r \times N_t}$ is the MIMO channel, $\mathbf{F} \in \mathbb{C}^{N_t \times L}$ is a linear precoder, and $\mathbf{x} \in \mathbb{C}^{L \times 1}$ is the transmitted symbol vector. The noise $\mathbf{n} \sim \mathcal{CN}(\mathbf{0}, \sigma_n^2 \mathbf{I}_{N_r})$ is additive white Gaussian noise. Although a flat-fading channel is assumed, this work can be extended to frequency-selective channels via orthogonal frequency-division multiplexing (OFDM), where each subcarrier experiences an equivalent flat-fading channel.

B. Probabilistic Shaping of QAM Symbols

Leveraging the fact that Gaussian signaling achieves capacity over the AWGN channel, we employ QAM symbols shaped by the PS method¹ [10], denoted as PS QAM symbols. A 2^{2M} -QAM symbol is constructed as the Cartesian product of two 2^M -PAM constellations, each with alphabet $\mathcal{O} = \{\pm 1, \pm 3, \dots, \pm(2^M - 1)\}$. Following [10], PS is applied to the PAM amplitudes, and the sign bits are assumed to be uniformly distributed. A constant composition distribution matcher (CCDM) [11] is adopted to map uniformly distributed data bits to shaped amplitude sequences according to a Maxwell–Boltzmann (MB) distribution

$$\mathbb{P}_\nu(s) = \frac{e^{-\nu \|s\|^2}}{\zeta}, \quad s \in \mathcal{O}, \quad (2)$$

where ν is the shaping parameter and $\zeta = \sum_{s' \in \mathcal{O}} e^{-\nu \|s'\|^2}$ is the normalization constant.

To satisfy the average transmit power constraint, the transmitted symbol vector is scaled as

$$\mathbf{x} = \alpha \mathbf{s}, \quad (3)$$

where $\mathbf{s} = [s_1, \dots, s_L]^\top$ is the symbol vector across the L spatial layers. The scaling factor $\alpha > 0$ is chosen such that $\mathbb{E}[|\alpha s_\ell|^2] = P_t/L$, where P_t is the total transmit power.

III. DISTRIBUTION-AWARE GMD TRANSCEIVER

Here, we propose a distribution-aware GMD transceiver for PS QAM symbols. First, we design an MAP detector with a VBLAST structure (MAP-VBLAST) in Section III-A and a BGMD precoder exploiting the PS priors in Section III-B. Then, we introduce the LC-MIMO mapping to enable SIC at CB level for mitigating error propagation in Section III-C.

¹Also known as probabilistic amplitude shaping, as in [10].

A. MAP-VBLAST Symbol Detection

We derive the MAP detection [12] for the PS QAM symbols, defined as

$$\hat{\mathbf{s}}_{map} = \arg \max_{\mathbf{s}} \{\ln \mathbb{P}(\mathbf{y}|\mathbf{s}) + \ln \mathbb{P}(\mathbf{s})\}, \quad (4)$$

where $\mathbb{P}(\mathbf{y}|\mathbf{s})$ is the conditional probability of the received signal given the transmitted symbol, and $\mathbb{P}(\mathbf{s})$ is the statistical prior of the transmitted symbols. Substituting the transmitted symbol vector in (3) into the signal model in (1), we have $\mathbf{y} = \alpha \mathbf{H}\mathbf{F}\mathbf{s} + \mathbf{n}$. With PS, the transmitted symbols follow the MB distribution $\mathbb{P}_\nu(\mathbf{s})$ in (2), which serves as the statistical prior (or PS priors), yielding $\ln \mathbb{P}(\mathbf{s}) = \ln \mathbb{P}_\nu(\mathbf{s}) = -\nu \|\mathbf{s}\|^2 - \ln \zeta$. Therefore, the MAP detection can be reformulated as

$$\hat{\mathbf{s}}_{map} = \arg \min_{\mathbf{s}} \left\{ \frac{\|\mathbf{y} - \alpha \mathbf{H}\mathbf{F}\mathbf{s}\|^2}{\sigma_n^2} + \nu \|\mathbf{s}\|^2 \right\} \quad (5)$$

$$= \arg \min_{\mathbf{s}} \left\{ \left\| \begin{bmatrix} \mathbf{y} \\ 0 \end{bmatrix} - \begin{bmatrix} \alpha \mathbf{H}\mathbf{F} \\ \sqrt{\sigma_n^2 \nu} \mathbf{I}_L \end{bmatrix} \mathbf{s} \right\|^2 \right\}. \quad (6)$$

Denoting the augmented channel matrix

$$\mathbf{G} = \begin{bmatrix} \alpha \mathbf{H}\mathbf{F} \\ \sqrt{\sigma_n^2 \nu} \mathbf{I}_L \end{bmatrix}, \quad (7)$$

we do the QR decomposition on \mathbf{G} , given by

$$\mathbf{G} = \mathbf{Q}_G \mathbf{R}_G \triangleq \begin{bmatrix} \mathbf{Q}_G^U \\ \mathbf{Q}_G^L \end{bmatrix} \mathbf{R}_G, \quad (8)$$

where \mathbf{Q}_G is an $(N_r + L) \times L$ matrix with orthonormal columns, \mathbf{Q}_G^U is an $N_r \times L$ matrix, and \mathbf{R}_G is an $L \times L$ upper triangular matrix with positive diagonal elements. The MAP detection of \mathbf{s} can be reformulated by multiplying $(\mathbf{Q}_G)^H$ on the objective function in (6), given by

$$\hat{\mathbf{s}}_{map} = \arg \min_{\mathbf{s}} \left\{ \|\tilde{\mathbf{y}} - \mathbf{R}_G \mathbf{s}\|^2 \right\} = \mathbf{R}_G^{-1} \tilde{\mathbf{y}}, \quad (9)$$

where $\tilde{\mathbf{y}} = [\tilde{y}_1, \dots, \tilde{y}_L]^\top = (\mathbf{Q}_G^U)^H \mathbf{y}$. With the upper-triangular matrix \mathbf{R}_G , we operate the VBLAST-like procedure involving sequential nulling and cancellation, with the detection order from layer L to layer 1, detailed as

$$\tilde{s}_{map,i} = \mathcal{M} \left(\frac{\tilde{y}_i - \sum_{j=i+1}^L [\mathbf{R}_G]_{i,j} \tilde{s}_{map,j}}{[\mathbf{R}_G]_{i,i}} \right), \quad (10)$$

from $i = L$ to $i = 1$, where $\tilde{s}_{map,i}$ denotes the i -th element of $\tilde{\mathbf{s}}_{map}$ and $[\mathbf{R}_G]_{i,j}$ represents the (i, j) -th element of \mathbf{R}_G . $\mathcal{M}(\cdot)$ denotes the symbol mapping in the QAM constellation.

B. Bayesian GMD Precoder

The primary challenge in VBLAST detection is its susceptibility to error propagation arising from SIC. Conventional approaches [13] mitigate this issue by optimizing the detection order based on post-detection SNR, at the cost of increased receiver complexity. In this subsection, we propose a BGMD precoder that equalizes the effective layer gains across layers, eliminating the need for optimal detection ordering. The resulting equal layer gains of BGMD also enable the use of a single-MCS scheme for low-complexity transmissions while

preserving channel capacity. Furthermore, by embedding PS priors into the precoder design, BGMD can provide enhanced throughput and decoding performance compared to conventional GMD-based designs [4], [5].

With the MAP detector in (9), we seek to design the BGMD precoder \mathbf{F} such that the diagonal elements of \mathbf{R}_G are equal. The SVD of the MIMO channel is given by $\mathbf{H} = \mathbf{U}\mathbf{S}\mathbf{V}^H$, where $\mathbf{U} \in \mathbb{C}^{N_r \times L}$ and $\mathbf{V} \in \mathbb{C}^{N_t \times L}$ are unitary matrices, and $\mathbf{S} \in \mathbb{R}^{L \times L}$ is a diagonal matrix with the singular values. We assume the BGMD precoder takes the form

$$\mathbf{F} = \mathbf{V}\mathbf{\Phi}^{1/2}\mathbf{\Omega}^H, \quad (11)$$

where $\mathbf{\Phi} = \text{Diag}\{\phi_1, \dots, \phi_L\}$ is the power-loading matrix, and $\mathbf{\Omega}$ is a unitary matrix to be designed for layer mixing. Substituting \mathbf{F} (as in (11)) into the augmented MIMO channel \mathbf{G} (as in (7)), we have

$$\mathbf{G} = \begin{bmatrix} \alpha \mathbf{U}\mathbf{S}\mathbf{\Phi}^{1/2}\mathbf{\Omega}^H \\ \sqrt{\sigma_n^2\nu}\mathbf{I}_L \end{bmatrix} \quad (12)$$

$$= \begin{bmatrix} \mathbf{I}_{N_r} & \mathbf{0} \\ \mathbf{0} & \mathbf{\Omega} \end{bmatrix} \begin{bmatrix} \alpha \mathbf{U}\mathbf{S}\mathbf{\Phi}^{1/2} \\ \sqrt{\sigma_n^2\nu}\mathbf{I}_L \end{bmatrix} \mathbf{\Omega}^H. \quad (13)$$

The second equation holds because $\mathbf{\Omega}$ is a unitary matrix. We apply the GMD [4] to the middle matrix in (13) as

$$\mathbf{B} \triangleq \begin{bmatrix} \alpha \mathbf{U}\mathbf{S}\mathbf{\Phi}^{1/2} \\ \sqrt{\sigma_n^2\nu}\mathbf{I}_L \end{bmatrix} = \mathbf{Q}_B \mathbf{R}_B \mathbf{P}_B^H, \quad (14)$$

where \mathbf{Q}_B is a semi-unitary matrix, \mathbf{P}_B is a unitary matrix, and \mathbf{R}_B is an upper triangular matrix whose diagonal elements are identical and equal to the geometric mean of the singular values of \mathbf{B} . By choosing $\mathbf{\Omega}^H = \mathbf{P}_B$ in (13), the augmented channel can be expressed as $\mathbf{G} = \tilde{\mathbf{Q}}\mathbf{R}_B$, where

$$\tilde{\mathbf{Q}} = \begin{bmatrix} \mathbf{I}_{N_r} & \mathbf{0} \\ \mathbf{0} & \mathbf{\Omega} \end{bmatrix} \mathbf{Q}_B. \quad (15)$$

Accordingly, the BGMD precoder is obtained by substituting $\mathbf{\Omega}^H = \mathbf{P}_B$ into (11), yielding $\mathbf{F} = \mathbf{V}\mathbf{\Phi}^{1/2}\mathbf{P}_B$. This BGMD precoder \mathbf{F} consists of the matrix \mathbf{V} for channel orthogonalization, the matrix $\mathbf{\Phi}$ for power-loading, and the unitary matrix \mathbf{P}_B for equalizing the effective subchannel gains. Since \mathbf{P}_B depends on the shaping parameter ν through (14), the BGMD precoder is explicitly distribution-aware.

C. Layer-Contained MIMO (LC-MIMO) and CB-SIC

Although the BGMD precoder equalizes the post-detection SNR across spatial layers and eliminates the need for optimal detection ordering in SIC, symbol detection errors may still occur during SIC. Symbol detection errors can propagate across layers during SIC and degrade decoding performance, potentially increasing overhead in the hybrid automatic repeat request process and retransmissions for reliable recovery.

To address this issue, LC-MIMO performs CW-to-layer mapping at the CB granularity, assigning each CB to a single spatial layer, rather than following the standardized 5G NR procedure that distributes coded bits across multiple layers [14]. Each CB is confined to a single spatial layer, enabling SIC to operate at the CB level instead of the coded-bit

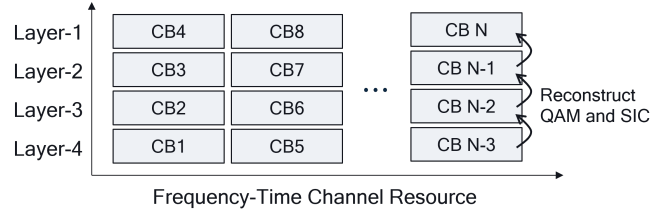


Fig. 1: LC-MIMO and the illustration of CB-SIC.

level. This allows the receiver to exploit the error-correction capability of channel coding to obtain more reliable symbol estimates and reduce error propagation in SIC.

The CB-SIC procedure operates as follows. First, the symbols corresponding to a CB on a specific layer are estimated and demapped into coded bits. These bits are then processed by a channel decoder (e.g., a LDPC decoder) to correct bit errors stemming from symbol detection errors. Subsequently, the decoded bits are re-encoded (e.g., by an LDPC encoder) and modulated to reconstruct the QAM symbols, providing significantly more reliable estimates. These reconstructed symbols are then subtracted from the received signal to cancel inter-layer interference. By performing interference cancellation using decoded and re-encoded symbols, rather than unreliable hard-symbol estimates, CB-SIC substantially reduces the likelihood of error propagation. LC-MIMO and the CB-SIC are illustrated in Fig. 1.

IV. NUMERICAL RESULTS

In this section, we evaluate the performance of the BGMD precoder and MAP-VBLAST detector, integrated with LC-MIMO mapping and CB-SIC, for the transmission of PS QAM symbols. We consider a single-user downlink MIMO transmission having $N_r = 4$ receiver antennas, $N_t = 4$ transmit antennas, and $L = 4$ spatial layers. We assume the 20 MHz TDL-A MIMO channel in 5G NR [15], corresponding to 48 resource blocks, each comprising 12 subcarriers at 30 kHz subcarrier spacing. The channel exhibits a 30 ns delay spread and an 11 Hz Doppler spread. The 5G NR low-density parity-check (LDPC) code [16] and the PS QAM symbol generation [10] are employed. The input data bits are generated by CCDFM [11], which follows an MB distribution with a shaping parameter ν , as defined in (2). We consider 64-QAM symbols shaped by PS with a shaping parameter ν and an LDPC code rate of 0.9258 for evaluation. Equal power allocation across the L layers is assumed. We assume that each transport block (TB) is transmitted within a single slot of duration $T_{\text{slot}} = 0.5$ ms and corresponds to a single CW. This CW is segmented into N_{cb} LDPC CBs, where each CB contains N_{cbit} coded bits determined by the 5G NR rate-matching procedure [16].

We consider the following baseline schemes for comparison. For transceiver design, the uniform channel decomposition (UCD) transceiver [5] is adopted as the baseline. This UCD transceiver represents the state-of-the-art GMD-based precoding with MMSE-VBLAST while not exploiting the PS priors.

For symbol detection, sphere decoding (SD) [9] is included as a benchmark. SD provides near maximum-likelihood detection performance but incurs higher computational complexity than linear detectors such as MAP or MMSE. Since LC-MIMO enables CB-SIC, we include a Hard-SIC scheme under NR-MIMO mapping as a benchmark to highlight the impact of error propagation, where Hard-SIC performs interference cancellation based on hard-symbol estimates. For CW-to-layer mapping, the mapping specified in 5G NR is used as a baseline, denoted as NR-MIMO [16].

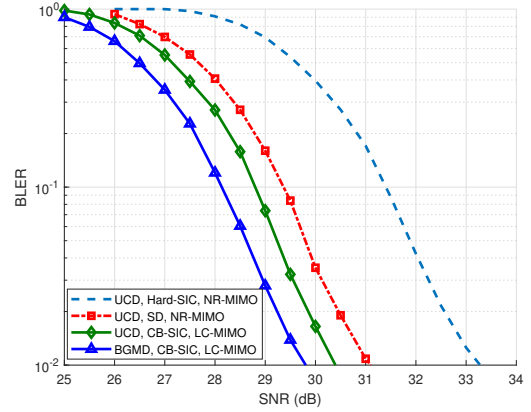
Fig. 2 presents the block error rate (BLER) versus SNR for various transceiver schemes and shaping parameters. The BLER corresponds to the CW error rate, where a CW is considered erroneous if any CB within the CW fails the cyclic redundancy check. The BLER monotonically decreases with increasing SNR across all evaluated schemes. In Fig. 2a ($\nu = 0.05$), we evaluate the BGMD with the CB-SIC in LC-MIMO against several benchmarks. For the UCD with CB-SIC in LC-MIMO, it achieves approximately SNR = 28.8 dB for 10% BLER, providing a 0.5 dB gain over the UCD with SD in NR-MIMO. This shows that CB-SIC in LC-MIMO can achieve a better performance with lower complexity than SD in NR-MIMO, when layer-mixing precoding is applied. The BGMD with CB-SIC in LC-MIMO further improves the required SNR to 28.1 dB, demonstrating the performance gains of distribution-aware precoding and symbol detection. Also, the UCD with Hard-SIC in NR-MIMO requires 31.2 dB to reach 10% BLER, showing a 3.1 dB degradation compared to the UCD with CB-SIC in LC-MIMO. This result validates that CB-SIC enabled in LC-MIMO effectively mitigates error propagation by leveraging the error-correction capability of the channel code, which facilitates SIC performance. Fig. 2b shows the results for a larger shaping parameter ($\nu = 0.1$). The performance trends of $\nu = 0.1$ are consistent with those of $\nu = 0.05$, but the gains from the distribution-aware design are more pronounced. UCD with CB-SIC achieves a 10% BLER at 26 dB, outperforming its Hard-SIC counterpart by 2 dB. Most notably, the proposed BGMD with CB-SIC achieves 10% BLER at only 24.5 dB. This shows a 1.3 dB gain over the BGMD with SD, effectively demonstrating that our proposed transceiver improves decoding reliability while significantly reducing demapper complexity compared to non-linear SD.

To compare the transceiver performance, we evaluate the empirical throughput versus SNR under different shaping parameters. The empirical throughput² is defined as

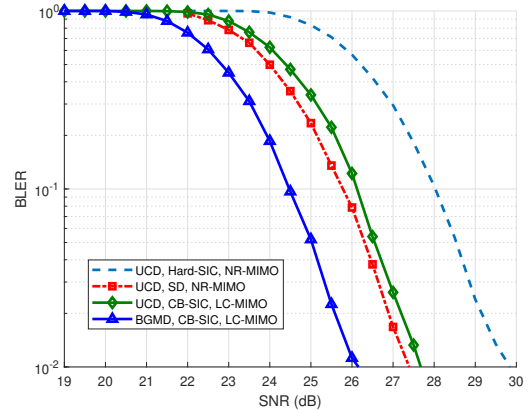
$$R_{QAM} = \frac{1}{T_{slot}} \left(N_{cb} H(\mathbf{x}) - \sum_{i=1}^{N_{cb}} \sum_{j=1}^{N_{cbit}} H_b(p_j^{(i)}) \right), \quad (16)$$

where $H(\mathbf{x})$ denotes the source entropy of the PS QAM symbols within one CB. $H_b(p) = -p \log_2 p - (1-p) \log_2 (1-p)$ is the binary entropy function. $p_j^{(i)}$ represents the posterior probability of the j -th coded bit in the i -th CB, obtained from its log-likelihood ratio (LLR) $\ell_j^{(i)}$ at the output of the equalizer,

²We impose the constraint of a fixed modulation order of 64 QAM.



(a) Shaping parameter $\nu = 0.05$.

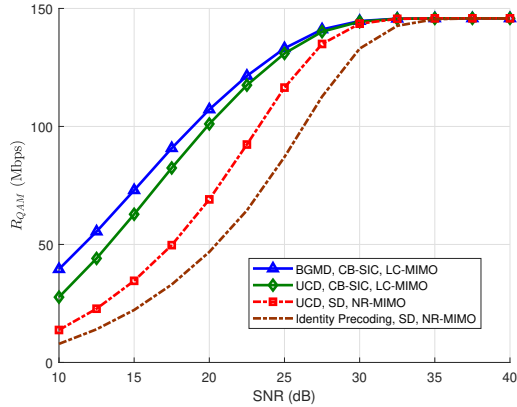


(b) Shaping parameter $\nu = 0.1$.

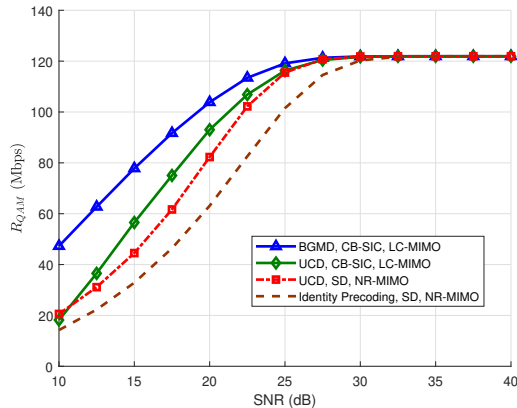
Fig. 2: BLER versus SNR.

i.e., $p_j^{(i)} = \left(1 + e^{-\ell_j^{(i)}}\right)^{-1}$. With the PS symbol structure [10], we have the source entropy per CB as $H(\mathbf{x}) = H(\mathbf{x}_{amp}) + H(\mathbf{x}_{sign})$, where $H(\mathbf{x}_{amp})$ and $H(\mathbf{x}_{sign})$ are the amplitude entropy and the sign entropy, respectively. The amplitude entropy is given by $H(\mathbf{x}_{amp}) = \frac{M_{amp}}{\log_2(Q)/2-1} H_\nu$, where M_{amp} is the number of amplitude bits per CB, $Q = 64$ for the 64-QAM modulation, and $H_\nu = -\sum_{s \in \mathcal{O}} \mathbb{P}_\nu(s) \log_2 \mathbb{P}_\nu(s)$ is the MB shaping entropy per amplitude symbol under the shaping parameter ν . Since the sign bits are assumed to be uniformly distributed and therefore each carries one bit of entropy, the sign entropy per CB is $H(\mathbf{x}_{sign}) = N_{cbit} - M_{amp}$.

Fig. 3 illustrates the empirical throughput versus SNR for shaping parameters $\nu = 0.05$ and $\nu = 0.1$. To evaluate the proposed BGMD transceiver, we compare its performance against the state-of-the-art UCD transceiver and identity precoding baselines. As shown in Fig. 3a ($\nu = 0.05$), identity precoding with SD in NR-MIMO requires SNR= 26 dB to achieve a throughput of 100 Mbps. Employing UCD with SD in NR-MIMO yields a 2 dB SNR gain. UCD with CB-SIC in LC-MIMO outperforms UCD with SD in NR-MIMO by 3dB at 100 Mbps, highlighting the benefits of inter-layer interference cancellation via CB-SIC. Notably, BGMD with CB-SIC consistently outperforms UCD with CB-SIC, demonstrating the



(a) Shaping parameter $\nu = 0.05$.



(b) Shaping parameter $\nu = 0.1$.

Fig. 3: Empirical throughput versus SNR.

advantage of incorporating PS priors in the transceiver design. Fig. 3b shows results for a larger shaping parameter ($\nu = 0.1$), where the overall performance trends remain consistent. The peak throughput decreases from 148 Mbps to 120 Mbps, as expected, due to the reduced source entropy under a larger PS shaping parameter. The gains from the distribution-aware transceiver become more pronounced: With CB-SIC, BGMD provides a 2-5 dB SNR gain over UCD. These results show that explicitly exploiting PS priors in transceiver design yields more significant gains as the PS symbol distribution deviates from the uniform constellation distribution.

V. CONCLUSION

This work proposed a distribution-aware GMD transceiver design that incorporates PS priors to enhance throughput and decoding performance in MIMO transmission. By leveraging the PS-induced symbol distribution, we derived an optimal MAP symbol detector and implemented it within a VBLAST detection framework. We developed a BGMD precoder to exploit PS priors in its design and equalize the per-layer post-detection SNR, enabling the use of a single-MCS transmission with reduced complexity while preserving channel capacity. In addition, we proposed a new CW-to-layer mapping

scheme, LC-MIMO mapping, to enable CB-SIC and mitigate cross-layer error propagation. Numerical results showed that the BGMD transceiver with LC-MIMO achieves significant gains in BLER and empirical throughput compared with state-of-the-art transceivers when PS QAM symbols are employed.

REFERENCES

- [1] C. G. Brinton, M. Chiang, K. T. Kim, D. J. Love, M. Beesley, M. Repeta, J. Roese, P. Beming, E. Ekudden, C. Li, G. Wu, N. Batra, A. Ghosh, V. Ziegler, T. Ji, R. Prakash, and J. Smee, "Key focus areas and enabling technologies for 6G," *IEEE Communications Magazine*, vol. 63, no. 3, pp. 84–91, 2025.
- [2] S. Hu, H. Wang, and S. Semenov, "Supporting probabilistic constellation shaping in 5G-NR evolution," *IEEE Trans. Wireless Commun.*, vol. 23, no. 4, pp. 3586–3599, 2023.
- [3] J. Fang, Q. Li, C. Chen, A. Gurevitz, and Y. Yoffe, "Probabilistic Shaping for Wi-Fi 8," *IEEE J. Sel. Areas Commun.*, vol. 43, no. 11, pp. 3708–3721, 2025.
- [4] Y. Jiang, J. Li, and W. W. Hager, "Joint transceiver design for MIMO communications using geometric mean decomposition," *IEEE Trans. Signal Process.*, vol. 53, no. 10, pp. 3791–3803, 2005.
- [5] —, "Uniform channel decomposition for MIMO communications," *IEEE Trans. Signal Process.*, vol. 53, no. 11, pp. 4083–4294, 2005.
- [6] F. Yang and Y. Dong, "Joint probabilistic shaping and beamforming scheme for MISO VLC systems," *IEEE Wireless Commun. Lett.*, vol. 11, no. 3, pp. 508–512, 2021.
- [7] W. Kang, "A Probabilistic Shaping Scheme for MIMO Systems with Signal Space Diversity," in *2022 IEEE Wireless Communications and Networking Conference (WCNC)*. IEEE, 2022, pp. 251–255.
- [8] K. Ivanov, W. Yang, and J. Jiang, "Probabilistic Shaping in MIMO: Going Beyond 1.53dB AWGN Gain With the Non-Linear Demapper," in *Proc. 13th Int. Symp. Topics in Coding (ISTC)*, 2025, pp. 1–5.
- [9] C. Studer, A. Burg, and H. Bolcskei, "Soft-output sphere decoding: Algorithms and VLSI implementation," *IEEE J. Sel. Areas Commun.*, vol. 26, no. 2, pp. 290–300, 2008.
- [10] G. Böcherer, F. Steiner, and P. Schulte, "Bandwidth efficient and rate-matched low-density parity-check coded modulation," *IEEE Trans. Commun.*, vol. 63, no. 12, pp. 4651–4665, 2015.
- [11] P. Schulte and G. Böcherer, "Constant composition distribution matching," *IEEE Trans. Inf. Theory*, vol. 62, no. 1, pp. 430–434, 2015.
- [12] S. M. Kay, *Fundamentals of Statistical Signal Processing: Estimation Theory*. USA: Prentice-Hall, Inc., 1993.
- [13] B. Hassibi, "An efficient square-root algorithm for BLAST," in *Proc. Int. Conf. ASSP*, vol. 2. IEEE, 2000, pp. 737–740.
- [14] 3GPP, "NR; Physical channels and modulation," Technical Specification (TS) 38.211, 02 2026, version 19.2.0.
- [15] —, "Study on channel model for frequencies from 0.5 to 100 GHz," Technical Report (TR) 38.901, 01 2024, version 17.1.0.
- [16] —, "NR; Multiplexing and channel coding," Technical Specification (TS) 38.212, 02 2026, version 19.2.0.